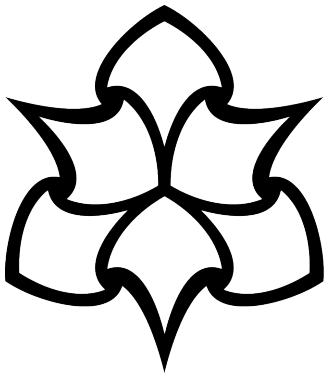

Nano Sized Zirconium Porphyrinic Metal-Organic Frameworks that Catalyze the Oxygen Reduction Reaction in Acid

Gan Chen, Michaela Burke Stevens, Yunzhi Liu, Laurie A. King, Jihye Park, Taeho Roy Kim, Robert Sinclair, Thomas F. Jaramillo, and Zhenan Bao**

G. Chen, Y. Liu, Prof. R. Sinclair
Department of Materials Science and Engineering, Stanford University, 496 Lomita Mall, Stanford, California 94305, United States

Dr. L. A. King
Faculty of Science and Engineering, Manchester Metropolitan University, Chester Street, Manchester, M1 5GD, UK.

Prof J. Park
Department of Chemistry, University of Colorado, Boulder, Colorado 80309, United States

Dr. T. R. Kim
Stanford Nano Shared Facilities, Stanford University, 348 Via Pueblo, Stanford, CA 94305, United States

Dr. M. Burke Stevens, Prof. T. F. Jaramillo, Prof. Z. Bao
Department of Chemical Engineering, Stanford University, 443 Via Ortega, Stanford, California 94305, United States
SUNCAT Center for Interface Science and Catalysis, SLAC National Accelerator Laboratory, 2575 Sand Hill Road, Menlo Park, California 94025, United States
E-mail: jaramillo@stanford.edu; zbao@stanford.edu

Keywords: Oxygen reduction reaction, electrocatalysis, porphyrinic metal–organic framework, coordination modulation, nanoparticle

Porphyrinic metal–organic frameworks (PMOFs) are very appealing electrocatalytic materials, in part, due to their highly porous backbone, well-defined and dispersed metal active sites, and their long-range order. Herein a series of (Co)PCN222 (PCN = porous coordination network) (nano)particles with different sizes are successfully prepared by coordination modulation synthesis. These particles exhibit stability in 0.1 M $HClO_4$ electrolyte with no obvious particle size nor compositional changes observed after being soaked for 3 days in the electrolyte or during

electrocatalysis. This long-term stability enables the in-depth investigation into the electrocatalytic oxygen reduction, and we further demonstrate that the (Co)PCN222 particle size correlates with its catalytic activity. Of the three particle sizes evaluated, (characteristic length scales of 200, 500, and 1000 nm), the smallest size demonstrates the highest mass activity while the largest size has the highest surface area normalized activity. Together these results highlight the importance of determining the structural stability of framework catalysts and provide insights into the important roles of particle size, opening new avenues to investigate and improve the electrocatalytic performance of this class of framework material.

Porphyrinic metal organic frameworks (PMOFs) have been recently studied in the photocatalysis of CO_2 reduction,[1-4] and as electrocatalysis of CO_2 reduction[5-9] and oxygen reduction.[10-13] Contrary to the majority of metal-nitrogen-carbon (M-N-C) catalysts derived from pyrolysis of nitrogen containing MOFs,[14] PMOF catalysts have well-defined MN_4 active sites, which are analogous to the well-defined nature of molecular catalysts. Indeed, the transition metal residing in the pocket of four nitrogen atoms within the porphyrin is thought to be the active sites for these catalysts.[8,13] The 3D architecture of MOFs is considered appealing for catalysis as the porosity could potentially facilitate diffusion of reactants throughout the pores and opens the door to the utilization of new active site motifs and enhanced catalytic activity.[15-17] Moreover, the hybrid nature of MOFs allows synthetic tunability, leading to MOFs of varying pore sizes and chemical environments. These pores provide potentially interesting confined environments for catalysis similar to those in enzymes. Such confined environments could potentially boost the catalyst performance if the pore structure is properly chosen.[18,19] Despite these appealing characteristics, electrocatalysts by nature require the facile movement of electrons (e.g. high electrical

conductivity) and limited examples of conductive MOFs are known in the literature.[13,20-22] Indeed, the intrinsically low conductivity of most PMOFs makes it challenging to access the majority of the active sites during electrocatalysis. Furthermore, compositional or structural solutions to enhance the conductivity of MOFs are challenging, however a lot of good electrocatalysts have intrinsically low conductivities. Therefore, understanding the role that morphology plays in catalysis (e.g. changing the particle size to increase electrochemical accessibility on the electrode surface) could give us new pathways to utilizing these unique active site motifs more efficiently. Beyond conductivity, the stability of MOFs under oxygen reduction reaction (ORR) relevant potentials in acidic media remains a challenge. Herein, we investigated the stability and catalytic activity of different sized porphyrinic MOFs, (Co)PCN222 (porous coordination network of $Zr_6(\mu_3\text{-}OH)_8(OH)_8(\text{Co-TCPP})_2$, also known as MOF-545)[23,24] for the ORR in an acidic electrolyte. Coordination modulation was applied to prepare (Co)PCN222 with different particle sizes ranging from 200 nm to 1000 nm in length. We show the successful integration of a CoN_4 active site motif ((Co)TCPP) into a 3D matrix and illustrate that the catalytic activity of these samples correlates with the particle size. We find that the (Co)PCN222 with the smallest particle size exhibited the highest mass activity while the largest size showed the highest surface area normalized activity. This work emphasizes the important role that particle size can play in electrocatalysis with MOFs that have low conductivities. Furthermore, it highlights Zr-based frameworks as a highly stable model system for designing new active site-motifs for the ORR or other electrochemical reactions.

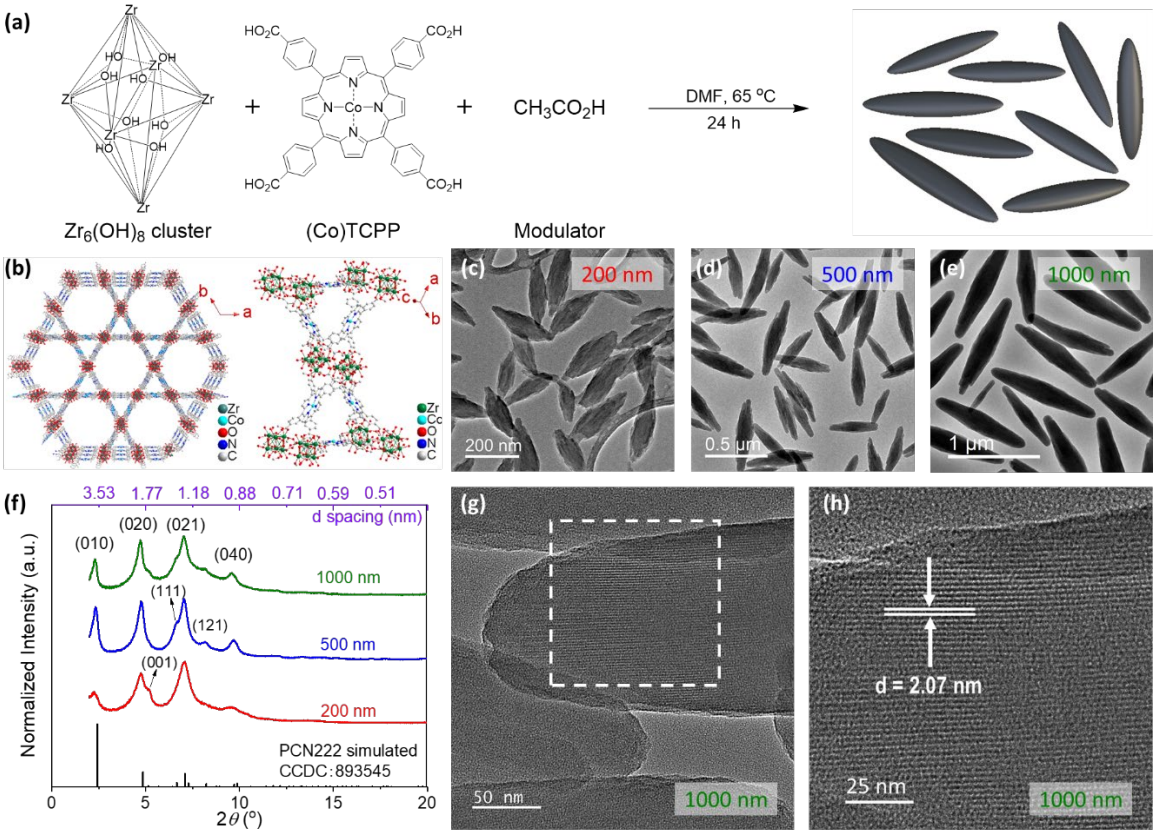

Figure 1. a) Synthetic scheme and b) crystal structure for (Co)PCN222 and corresponding characterization for as synthesized (Co)PCN222 (nano)particles with a nominal length of 200 nm (red), 500 nm (blue), and 1000 nm (green) via c-e) Bright field (BF)-TEM images of 200, 500, 1000 nm particles; f) PXRD and g,h) High resolution TEM images of 1000 nm particles.

The (Co)PCN222 particles were prepared by adapting the solvothermal synthesis from previous works.[24,25] As shown in **Figure 1**a, acetic acid was used as the coordination modulator. In the reaction, acetic acid competes with the porphyrin ligand in coordination with Zr clusters and thus slower nucleation and growth of MOF is expected. In general, more coordination modulators lead to fewer and larger particles that have higher crystallinity.[26-31] This rationale is confirmed in our synthesis, which confirms that more coordination modulator leads to larger particles. Specifically, synthesis with 0.70, 0.87 and 1.05 M of acetic acid gave tapered rod-like particles of length-scales around 200, 500 and 1000 nm (Figure 1c-e) along the major axis (detailed particle size and size distribution is given in Table S1). Powder X-ray Diffraction (PXRD) of the three samples (Figure

1f) corresponds well with the simulated patterns from reported PCN222 crystal structure. Note it is not trivial to interpret PXRD on these (nano)particles as crystallinity quantification was found to be influenced by how the nanoparticle dispersions were dried, e.g., the rotation rate in rotary evaporation determines whether the smaller peaks can be observed by PXRD (Figure S3). High resolution TEM (HR TEM) further supports the high degree of crystallinity of these particles and the 1000 nm particle appears to be largely single-crystalline (Figure 1g, h, Figure S6). A lattice d-spacing along the arrowed direction in Figure 1h is determined to be 2.07 nm, which is very close to the expected d-spacing for (110) planes (2.10 nm, Table S2). These (110) planes are parallel to the major axis of the tapered rods. Based on PCN222's crystal structure (Figure 1b), (110) planes are parallel to the open 1D channels in this MOF, indicating the 1D channels also aligns with the major axis of these particles. Note that due to the low structure factor for (110) plane (Table S2) and the small particle size of our samples, the (110) peak was not observed in our PXRD. Consistent with its low structure factor, the diffraction of the (110) planes is too weak to be observed in selected area diffraction pattern (SADP) (Figure S7). Although (110) diffraction is weak, the (110) planes do show the periodicity of the open pores, which is often prominent in high resolution TEM images of crystal structures. From HR TEM both the 200 nm and 500 nm particles appear to be poly-crystalline (Figure S4, S5), however it is worth noting that smaller particles could be more sensitive to e-beam damage. Additionally, the particles will be damaged when trying to obtain an Energy Dispersive X-ray Spectroscopy (EDS) using a smaller beam focused on the particles (Figure S8, S9). Even with the beam damage during the EDS acquisition, EDS was acquired for the 1000 nm sample (Figure S9) to check the elemental composition at different locations of a particle. No significant variations were observed in EDS graph between each

position. Also, the signal intensity ratios between the Zr and Co are compared to check for any inhomogeneity (Figure S9e), which we did not find.

One of the major concerns with using MOFs in any kind of application is the durability of their framework structure. Zr-based MOFs are well known for their high structural stability which has been attributed to the strong coordination bonds between Zr(IV) and carboxylate groups that hold the porous network together. (Fe)PCN-222 MOF has previously shown extraordinary tolerance to concentrated HCl and retained bulk crystallinity, as seen by PXRD, even after soaking for 24 h.[24] To further examine the extent of stability for (Co)PCN222 particles, we coupled TEM and PXRD analysis to characterize the change in particle size and structure as a function of soaking time in 0.1 M $HClO_4$, a common electrolyte employed in studying catalysts for ORR.[32] The particles were soaked in the electrolyte for up to 3 days, and no obvious changes to the particle shape were observed by TEM (**Figure 2**a, b, e, f). Furthermore, PXRD (Figure 2d, h) shows that the crystallinity of both the 200 nm and 1000 nm particles is also retained after the acid soak. Quantitative analysis of particle size, averaging over 100 particles (Figure S10-15),[33,34] however, indicates that while there are no bulk changes, the soaking did impact the particle size slightly. For the 200 nm particles, both the major axis (length) and the minor axis (width) of the tapered rods increased by approximately 20% after being soaked in the electrolyte for one day, with their length increasing from 217 ± 50 nm to 258 ± 40 nm and their width from 73 ± 16 nm to 90 ± 14 nm. These dimensions remained similar after two additional days of soaking: 251 ± 41 nm and 88 ± 13 nm, respectively. However, for the 1000 nm particles, the length decreased ~ 6 % after day one, and ~ 8 % overall after three days while the width increased by ~ 14 % during the three days of soaking. Increased dimensions due to soaking could result from pore expansion induced by water

and/or ClO_4^- absorption[35] while the size decrease could be attributed to dissolution of the MOF structure. As shown in Figure 1g, the 1000 nm sample is nearly single-crystalline and the open channels align with the major axis, this could influence the ion intercalation. Interestingly, morphological changes at the tips are more pronounced than within the main body of the tapered rods. This is revealed by the decrease in length and rounded tips observed by TEM imaging (Figure S10-15). These tip-specific changes could be attributed to the geometry of tapered rod-like structure exposing the tip edges to a larger volume of acidic electrolyte and/or faster electrolyte diffusion into the open channels of the 1D MOF channels, which are aligned to have openings at the tips. BET was further used to examine the change in posorsity during the soak experiment. The 200 nm sample was investigated and gave an almost identical surface area and pore size distribution (Figure S16) after 3 days' soak in 0.1 M $HClO_4$, further demonstrating the framework's stability in acid.

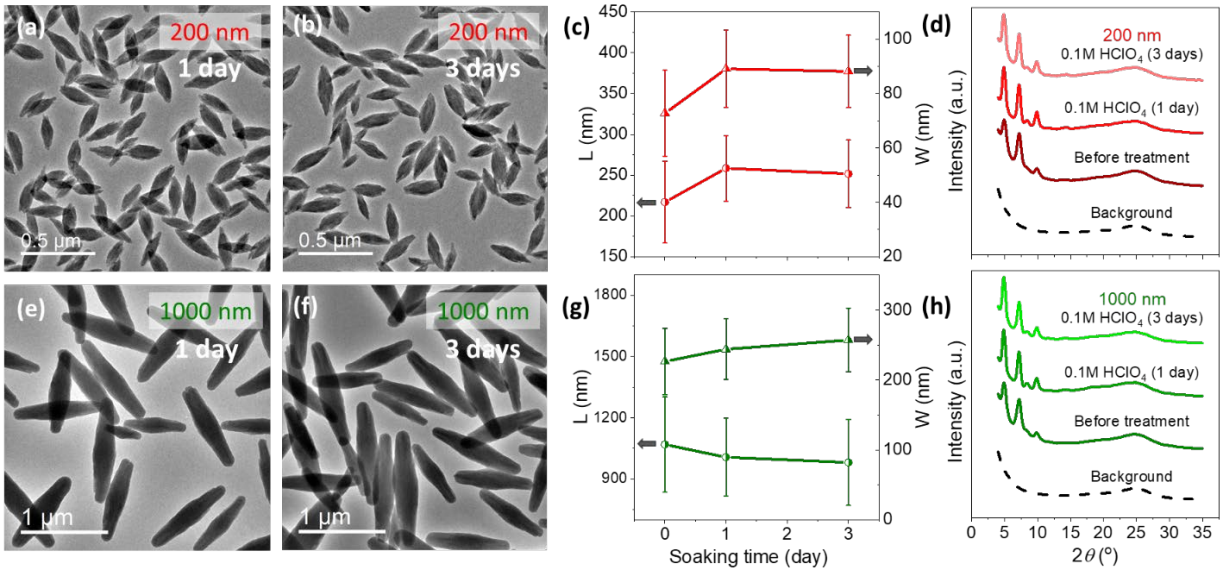

Figure 2. BF-TEM images for 200, 1000 nm (Co)PCN222 after being soaked in 0.1 M $HClO_4$ for 1 day (a and e, respectively) and 3 days (b and f, respectively). c, g) Particle size measured from TEM images based on the particle length (L, left) and width (W, right) and d,h) PXRD for as

synthesized 200 and 1000 nm (Co)PCN222 as a function of time during soaking. PXRD was collected on (Co)PCN222 samples mixed with Vulcan carbon.

While these morphological changes are notable, the overall stability of the (Co)PCN222 in 0.1M $HClO_4$ electrolyte is evident, allowing for the samples to be further evaluated for their catalytic activity for the ORR. Due to their large particle size and low conductivity, for electrochemical studies, the PNC222 particles were dispersed in a high weight (90 w/w%) percent of conductive Vulcan carbon support, using Nafion as a binder. This reflects a modified version of conventional electrode preparations commonly used for Pt catalysts in acid, employing a higher carbon content in our particular case in order to facilitate electron transport in catalysts with low conductivities.[36]

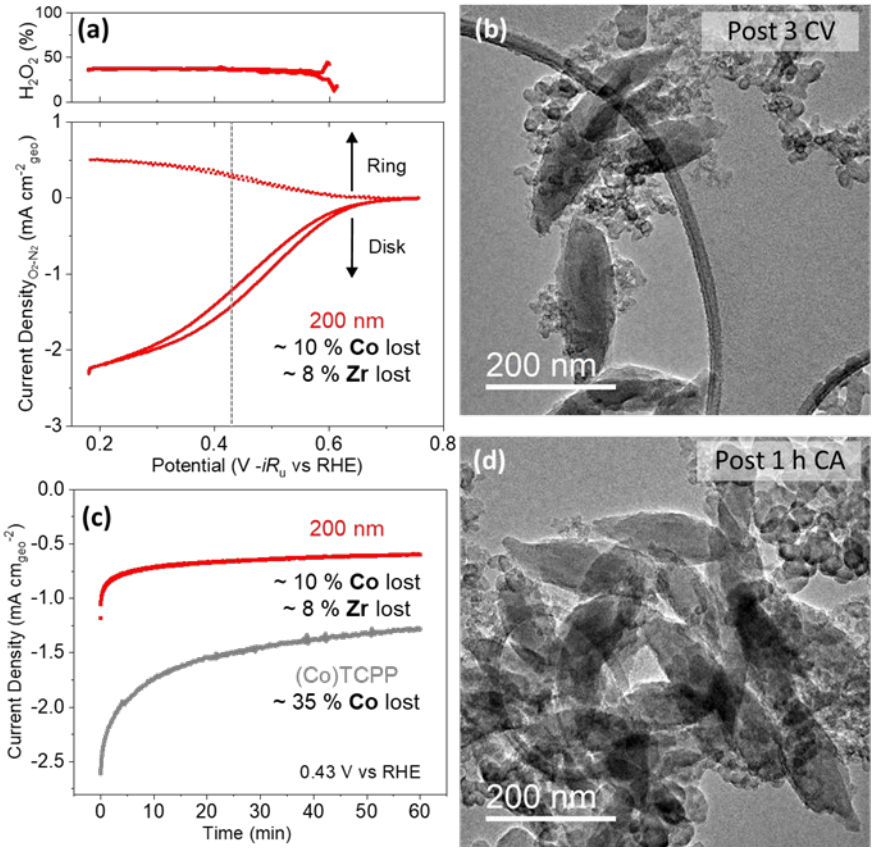

Figure 3. Electrochemical selectivity and stability evaluation of 200 nm (Co)PCN222 particles (red) compared to (Co)TCPP (grey). a) Cyclic voltammograms (third cycle, 20 mV s^{-1}) in and RRDE configuration (Pt ring,) showing disk current, ring current (normalized by the collection efficiency (~ 4x)), and subsequent H_2O_2 selectivity (top) with b) corresponding BF-TEM images for the 200 nm (Co)PCN222 particles after voltammetry, the smaller particles are Vulcan carbon. Voltammetry current has been corrected by the catalyst's current in N_2 saturated electrolyte. Longer-term stability evaluation at c) 1h polarization at 0.43 V vs RHE and d) corresponding BF-TEM images of the 200 nm (Co)PCN222 after 1 h of the applied potential, the smaller particles are Vulcan carbon. Co and Zr dissolution during electrochemistry was evaluated by quantifying the amount of Co and Zr remaining at the end of the measurement (ICP-OES) and is noted as % Co or Zr lost. All measurements performed on GC disk electrodes in O_2 saturated 0.1 M $HClO_4$ electrolyte at a rotation of 1600 rpm.

The initial electrochemical stability and selectivity of the 200 nm (Co)PCN222 particles is summarized in **Figure 3**a and b. The 200 nm (Co)PCN222 sample onsets (0.1 mA cm_{geo}^{-2}) for the ORR at 0.64 ± 0.01 V vs RHE. This current can be attributed to both 4 e^- and 2 e^- process based on the full or partial reduction of O_2 to H_2O or H_2O_2, respectively. The H_2O_2 production, as measured by a rotating ring disk electrode (RRDE) appears to onset almost simultaneously with 4 e^- reduction and the catalyst has a maximum H_2O_2 selectivity of 37.5%, while exhibiting a limiting current of 2.25 mA cm^{-2}. This low limiting current is likely due to the low loading of active materials relative to the geometric surface area of the electrode, due to the need for substantial amounts of Vulcan carbon. This complicates a direct comparison of the activity of these (Co)PCN222 particles to other systems, and as such any comparisons should be done with care,

focusing on the activity normalized by Co loading or surface area in the current regime that is dominated by the catalyst kinetics. Using ICP-OES analysis to determine the amount of Co and Zr remaining on the electrode after catalysis we see that the catalysts lose ~ 10 % Co and 8 % Zr during electrochemical cycling (e.g. 3 cycles in an O_2 saturated electrolyte and 4 cycles in a N_2 saturated electrolyte). The proportional loss of Co and Zr suggests that the mechanism for degradation is either the loss of a very small number of particles or degradation of the particle edges. Post-catalysis TEM (Figure 3b) shows almost unchanged particle size and morphology. This unchanged size supports the mechanism for degradation as the loss of particles from the Vulcan carbon, however more quantitative TEM would be needed to ascertain changes to the particle edges.

To further evaluate the longer-term stability during the ORR, the 200 nm (Co)PCN222 particles were polarized at 0.43 V vs RHE for 1 h (Figure 3c). As can be seen in Figure 3c, the current density dropped quickly from -1.18 mA cm^{-2} to -0.8 mA cm^{-2} and within 3 min the catalyst has lost ~ 30 % of its activity. After the initial current loss, the current density largely stabilizes ending at -0.6 mA cm^{-2} after an hour of testing. ICP-OES studies of the electrodes after this hour-long evaluation reveal that the samples only lost ~ 10 % and 8 % of Zr and Co, respectively. This is approximately the same amount lost during the voltammetry stability tests and could indicate that for these samples, regardless of electrochemical analysis, there is an initial fast detachment of particles that are not well adhered to the conductive carbon support. Furthermore, the TEM (Figure 3d) exhibits almost unchanged particle size and morphology after 1 h. The lack in material degradation with ~ 50 % current loss could indicate that there is some sort of active-site specific deactivation or that the lost ~ 10 % Co sites contribute ~ 50 % of the reduction current and not all

the particles on the electrode have the same accessibility for ORR . Alternatively, the (Co)TCPP control lost ~ 45 % of its current with ~ 35 % loss in Co over 1 h of testing. This could indicate an electrocatalytic degradation mechanism that is a mix between porphyrin detachment from the electrode[37] and CoN_4 active site deactivation. Furthermore, it is likely that the (Co)TCPP have different accessibility for ORR than the (Co)PCN222 particles. It is interesting to note that under these conditions the Zr-coordinated networks did moderately enhance the chemical or mechanical stability of the (Co)TCPP within this system. Overall these results demonstrate the promising structural stability of (Co)PCN222 in this working environment and motivate further study of electrochemical degradation pathways.

In order to probe the role that particle size plays on the activity of (Co)PCN222, three samples with particle sizes of 200 nm, 500 nm, and 1000 nm were compared using cyclic voltammetry (**Figure 4**a). Because the high loading of conductive support (90 w/w% Vulcan), low catalyst distribution, and differences in catalyst surface area complicate a conventional evaluation of current density normalized by the geometric surface area of the electrode, the current density was normalized by the total Co content on the surface of the electrode. After this normalization, all of the particle sizes exhibit a similar ORR onset (0.1 mA cm^{-2}), suggesting that the same CoN_4 active site motif is maintained across all particle sizes. Notably, this common onset potential for the different particles is > 50 mV more negative than that of the control (Co)TCPP sample. This difference in performance between the (Co)TCCP and (Co)PCN222 is likely due to the large differences in electrochemically available Co-sites that stem from comparing a molecular catalyst (that is essentially embedded into the Vulcan carbon) to particles with large dimensions on the

order of ~ 100-1000 nm. For the purpose of our particle size comparison, we evaluated the activity as a function of total Co and total catalyst surface area (see Figure S17 for calculation).

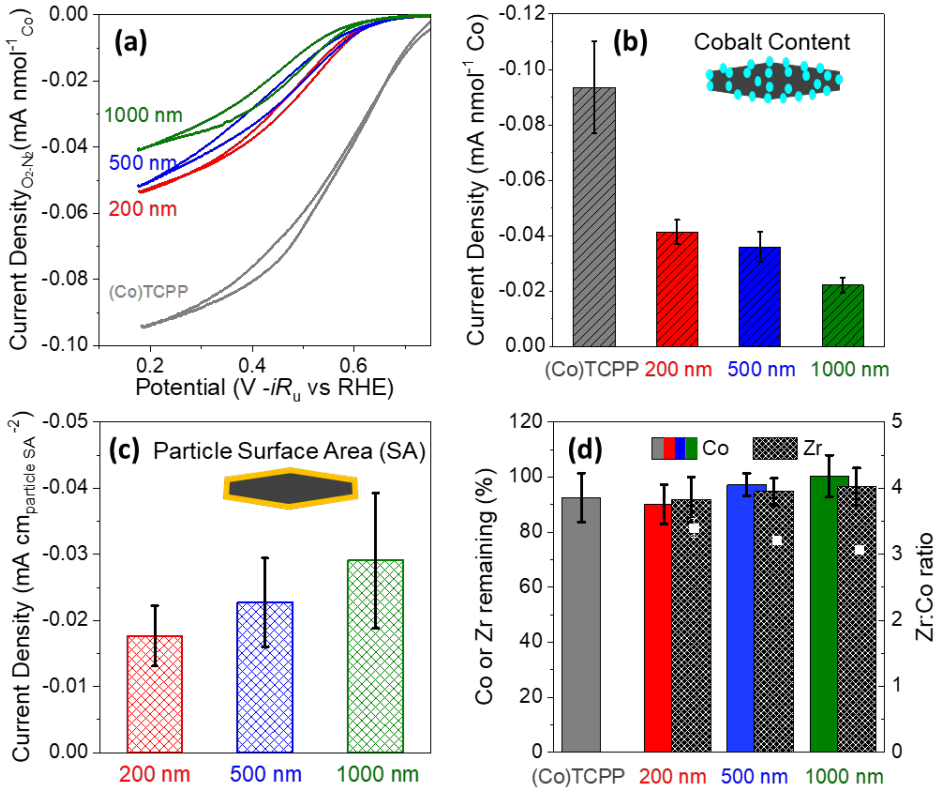

Figure 4. Electrochemical performance evaluation of 200, 500, 1000 nm (Co)PCN222 particles using cyclic voltammetry (third cycle, 20 mV s^{-1}, 1600 rpm, O_2 saturated 0.1 M $HClO_4$) with the a) full voltammogram normalized by total Co content and the current of reverse sweep at 0.43 V vs RHE normalized by b) Co content and c) total particle surface area (see SI calculations Figure S17) and d) total ICP-OES results for post-catalysis samples after cycling in nitrogen and oxygen (4 and 3 cycles, respectively). All data has been corrected by the catalyst's current in N_2 saturated electrolyte (Figure S18).

As seen in Figure 4b, when normalized by total Co content (ICP-OES), the smaller particle sizes demonstrate higher ORR activity and the current densities at 0.43 V vs RHE trend as follows for

200 nm, 500 nm, and 1000 nm: -0.043 ± 0.004, -0.036 ± 0.005, and -0.022 ± 0.003 mA nmol Co^{-1} (See Table S3). We hypothesize that these performance differences originate from the intrinsically low conductivities of the catalysts being tested. This is amplified by the fact that this Co normalization assumes that all the CoN_4 sites are active. However, due to their intrinsically low conductivity, it is likely that only the surface layers that are in good contact with conductive carbon will have access to electrons that catalyze the reaction. Therefore, because the smaller particles have a higher specific surface area and likely a greater fraction of CoN_4 on the surface, the 200 nm particles outperform the 1000 nm particles because more of the Co-sites are participating in the ORR. To evaluate the activity of the CoN_4 sites only on the surface of the particle, we normalized by the total particle surface area (**Equation 1**). Generally, electrochemical double layer capacitance (EDLC) measurements are performed to normalize by catalyst surface area, however this was not possible due to the high Vulcan carbon content (Figure S18). Therefore, the approximate (Co)PCN222 particle surface area (SA) in this case is a mathematical approximation of the total catalyst surface area based on Co content (ICP-OES), crystal structure information, and particle size and geometry (Figure S17).

$$Current\ Density\ (mA\ cm^{-2}_{particle\ SA}) = \frac{ORR\ current}{Approximate\ (Co)PCN222\ particle\ SA} \quad (1)$$

Comparing the current density normalized by (Co)PCN222 surface area (Figure 4c), we see slight differences between each particle size with the 1000 nm samples exhibiting the highest performance. This could indicate that the 1000 nm particles have an intrinsically higher surface activity than the smaller particles. However, a main assumption in this activity normalization (by particle surface area, Equation 1) is that every Co-site on the outer surface is active. Similar to the normalization by total Co content in Figure 4b, this is still likely an over estimation. Therefore, differences in performance could also indicate differences in contact between the (Co)PCN222

particles and the carbon support could be due to differences in particle aggregation. This further highlights the importance of understanding the morphology of the of electrochemical surface in in order to compare the activity of complicated catalysts. SEM on the electrodes made with 200 nm and 1000 nm samples shows that 1000 nm particles distribute homogenously in Vulcan carbon while there is evidence for aggregation in the 200 nm sample (Figure S19). It is likely that this particle aggregation and change in the morphology of the active surface leads to less accessible (Co)PCN222 surface areas and therefore lower ORR performance. For future studies interested in evaluating enhanced activity via confinement it will be necessary to develop advanced active-site normalization and detection techniques.

Post-catalysis characterizations of all particles were done using via ICP-OES analysis to examine the (Co)PCN222 particles' stability in 0.1M $HClO_4$ electrolyte under reductive potentials. After three cycles of CV, of the three particle sizes, the 1000 nm sample exhibited the best nominal stability. However, even for the least stable 200 nm sample, ≥ 90 % Co and 92 % Zr remained, reflecting good stability of (Co)PCN222 under reductive potentials. Among the three samples investigated, the 200 nm sample had the highest mass normalized current density while remaining stable. Based on these conclusions, future work on 3D frameworks should focus on designing easy-to-synthesize, stable, and small particles when pursing electrocatalysts with low conductivities.

In summary, we demonstrated that the (Co)PCN222 (nano)particles prepared by coordination modulation exhibit activity and stability for the oxygen reduction reaction in acid, opening new opportunities to investigate and improve the electrocatalytic performance of this class of framework material. The ORR activity of these particles is found to correlate with particle size.

The smallest particles (200 nm) we tested exhibited the highest oxygen reduction current per Co atom in ORR, likely due to the higher specific surface area, however they also exhibited the lowest current per total particle surface area. Our work shows that the particle size and the morphology of the electrochemically active surface (e.g. from aggregation of particles) can play important roles in determining the catalytic performances for catalysts with low conductivities and provides fundamental guidance on using framework materials broadly in electrocatalysis.

Supporting Information
Supporting Information is available from the Wiley Online Library or from the author.

Acknowledgements
G.C. and M.B.S. contributed equally to this work. This work was funded by the Toyota Research Institute. This work was done as a part of the SUNCAT Center for Interface Science and Catalysis which is supported by the U.S. Department of Energy and Basic Energy Sciences. Part of this work was performed at the Stanford Nano Shared Facilities (SNSF)/Stanford Nanofabrication Facility (SNF), supported by the National Science Foundation under award ECCS-1542152. The authors thank Dr. Guangchao Li in the Environmental Measurements Facility for the acquisition of ICP-OES data.

Received: ((will be filled in by the editorial staff))
Revised: ((will be filled in by the editorial staff))
Published online: ((will be filled in by the editorial staff))

References

[1]. Fang, X.; Shang, Q.; Wang, Y.; Jiao, L.; Yao, T.; Li, Y.; Zhang, Q.; Luo, Y.; Jiang, H.-L., *Adv. Mater.* **2018,** *30* (7), 1705112.
[2]. Xu, H.-Q.; Hu, J.; Wang, D.; Li, Z.; Zhang, Q.; Luo, Y.; Yu, S.-H.; Jiang, H.-L., *J. Am. Chem. Soc.* **2015,** *137* (42), 13440.
[3]. Zhang, H.; Wei, J.; Dong, J.; Liu, G.; Shi, L.; An, P.; Zhao, G.; Kong, J.; Wang, X.; Meng, X.; Zhang, J.; Ye, J., *Angew. Chem. Int. Ed.* **2016,** *55* (46), 14310.
[4]. Sadeghi, N.; Sharifnia, S.; Do, T.-O., *J. Mater. Chem. A* **2018,** *6* (37), 18031.
[5]. Dong, B.-X.; Qian, S.-L.; Bu, F.-Y.; Wu, Y.-C.; Feng, L.-G.; Teng, Y.-L.; Liu, W.-L.; Li, Z.-W., *ACS Appl. Energy Mater.* **2018,** *1* (9), 4662.
[6]. Matheu, R.; Gutierrez-Puebla, E.; Monge, M. Á.; Diercks, C. S.; Kang, J.; Prévot, M. S.; Pei, X.; Hanikel, N.; Zhang, B.; Yang, P.; Yaghi, O. M., *J. Am. Chem. Soc.* **2019,** *141* (43), 17081.

[7]. Hod, I.; Sampson, M. D.; Deria, P.; Kubiak, C. P.; Farha, O. K.; Hupp, J. T., *ACS Catal.* **2015,** *5* (11), 6302.
[8]. Kornienko, N.; Zhao, Y.; Kley, C. S.; Zhu, C.; Kim, D.; Lin, S.; Chang, C. J.; Yaghi, O. M.; Yang, P., *J. Am. Chem. Soc.* **2015,** *137* (44), 14129.
[9]. Wang, Y.-R.; Huang, Q.; He, C.-T.; Chen, Y.; Liu, J.; Shen, F.-C.; Lan, Y.-Q., *Nat. Commun.* **2018,** *9* (1), 4466.
[10]. Lions, M.; Tommasino, J. B.; Chattot, R.; Abeykoon, B.; Guillou, N.; Devic, T.; Demessence, A.; Cardenas, L.; Maillard, F.; Fateeva, A., *Chem. Commun.* **2017,** *53* (48), 6496.
[11]. Usov, P. M.; Huffman, B.; Epley, C. C.; Kessinger, M. C.; Zhu, J.; Maza, W. A.; Morris, A. J., *ACS Appl. Mat. Interfaces* **2017,** *9* (39), 33539.
[12]. Jahan, M.; Bao, Q.; Loh, K. P., *J. Am. Chem. Soc.* **2012,** *134* (15), 6707.
[13]. Zhong, H.; Ly, K. H.; Wang, M.; Krupskaya, Y.; Han, X.; Zhang, J.; Zhang, J.; Kataev, V.; Büchner, B.; Weidinger, I. M.; Kaskel, S.; Liu, P.; Chen, M.; Dong, R.; Feng, X., *Angew. Chem. Int. Ed.* **2019,** *58* (31), 10677.
[14]. Hua, X.; Luo, J.; Shen, C.; Chen, S., *Catal. Sci. Technol.* **2018,** *8* (7), 1945.
[15]. Lu, X. F.; Xia, B. Y.; Zang, S.-Q.; Lou, X. W., *Angew. Chem. Int. Ed*. **2020,** *59* (12), 4634.
[16]. Downes, C. A.; Marinescu, S. C., *ChemSusChem* **2017,** *10* (22), 4374.
[17]. Aiyappa, H. B.; Masa, J.; Andronescu, C.; Muhler, M.; Fischer, R. A.; Schuhmann, W., *Small Methods* **2019,** *3* (8), 1800415.
[18]. Montoya, J. H.; Seitz, L. C.; Chakthranont, P.; Vojvodic, A.; Jaramillo, T. F.; Nørskov, J. K., *Nat. Mater.* **2017,** *16* (1), 70.
[19]. Kulkarni, A.; Siahrostami, S.; Patel, A.; Nørskov, J. K., *Chem. Rev.* **2018,** *118* (5), 2302.
[20]. Yoon, H.; Lee, S.; Oh, S.; Park, H.; Choi, S.; Oh, M., *Small* **2019,** *15* (17), 1805232.
[21]. Miner, E. M.; Wang, L.; Dincă, M., *Chem. Sci.* **2018,** *9* (29), 6286.
[22]. Miner, E. M.; Gul, S.; Ricke, N. D.; Pastor, E.; Yano, J.; Yachandra, V. K.; Van Voorhis, T.; Dincă, M., *ACS Catal.* **2017,** *7* (11), 7726.
[23]. Morris, W.; Volosskiy, B.; Demir, S.; Gándara, F.; McGrier, P. L.; Furukawa, H.; Cascio, D.; Stoddart, J. F.; Yaghi, O. M., *Inorg. Chem.* **2012,** *51* (12), 6443.
[24]. Feng, D.; Gu, Z.-Y.; Li, J.-R.; Jiang, H.-L.; Wei, Z.; Zhou, H.-C., *Angew. Chem. Int. Ed.* **2012,** *51* (41), 10307.
[25]. Bůžek, D.; Zelenka, J.; Ulbrich, P.; Ruml, T.; Křížová, I.; Lang, J.; Kubát, P.; Demel, J.; Kirakci, K.; Lang, K., *J. Mater. Chem. B* **2017,** *5* (9), 1815.
[26]. Tsuruoka, T.; Furukawa, S.; Takashima, Y.; Yoshida, K.; Isoda, S.; Kitagawa, S., *Angew. Chem. Int. Ed.* **2009,** *48* (26), 4739.
[27]. Diring, S.; Furukawa, S.; Takashima, Y.; Tsuruoka, T.; Kitagawa, S., *Chem. Mater.* **2010,** *22* (16), 4531.
[28]. Han, Y.; Liu, M.; Li, K.; Zuo, Y.; Wei, Y.; Xu, S.; Zhang, G.; Song, C.; Zhang, Z.; Guo, X., *CrystEngComm* **2015**, *17* (33), 6434.
[29]. He, C.; Lu, K.; Liu, D.; Lin, W., *J. Am. Chem. Soc.* **2014**, *136* (14), 5181.
[30]. Lu, K.; He, C.; Lin, W., *J. Am. Chem. Soc.* **2014**, *136* (48), 16712.
[31]. Park, J.; Jiang, Q.; Feng, D.; Mao, L.; Zhou, H.-C., *J. Am. Chem. Soc.* **2016**, *138* (10), 3518.
[32]. Stamenković, V.; Schmidt, T. J.; Ross, P. N.; Marković, N. M., *J. Phys. Chem. B* **2002,** *106* (46), 11970.
[33]. Carpenter, D. T.; Rickman, J. M.; Barmak, K., *J. Appl. Phys.* **1998**, *84* (11), 5843.

[34]. Park, D.-W.; Sinclair, R.; Lal, B. B.; Malhotra, S. S.; Russak, M. A., *J. Appl. Phys.* **2000**, *87* (9), 5687.
[35]. Parent, L. R.; Pham, C. H.; Patterson, J. P.; Denny, M. S.; Cohen, S. M.; Gianneschi, N. C.; Paesani, F., *J. Am. Chem. Soc.* **2017,** *139* (40), 13973.
[36]. Shinozaki, K.; Zack, J. W.; Richards, R. M.; Pivovar, B. S.; Kocha, S. S., *J. Electrochem. Soc.* **2015,** *162* (10), F1144.
[37]. Collman, J. P.; Denisevich, P.; Konai, Y.; Marrocco, M.; Koval, C.; Anson, F. C., *J. Am. Chem. Soc.* **1980,** *102* (19), 6027.

Zirconium porphyrinic metal-organic framework (Co)PCN222 (nano)particles show good stability and activity in catalyzing oxygen reduction reaction in acidic $HClO_4$ electrolyte. These particles exhibit enhanced mass activity within smaller particles whereas higher catalyst surface area normalized activity within larger particles.

Oxygen reduction reaction, electrocatalysis, porphyrinic metal–organic framework, coordination modulation, nanoparticle

G. Chen, M. Burke Stevens, Y. Liu, L. A. King, J. Park, T. R. Kim, R. Sinclair, T. F. Jaramillo*, and Z. Bao*

Nano Sized Zirconium Porphyrinic Metal-Organic Frameworks that Catalyze the Oxygen Reduction Reaction in Acid

ToC figure ((Please choose one size: 55 mm broad × 50 mm high or 110 mm broad × 20 mm high. Please do not use any other dimensions))